Abbreviated Key Title: Glob. J. Environ. Sci. Technol.
ISSN: 2384-5058 (Print) & Open Access
Vol. 12(2): Pp. 51-61, April, 2024.
DOI:10.54978
Global Journal of Environmental Science and Technology: ISSN-2360-7955, (Print) & Open Access
Volume-12 | Issue-4 | April, 2024 | Research Paper

Analytical Modelling of Hardness as a non-elastic performance factor in augmenting the Structural Integrity of Pipeline Weldment

Mabiaku Timothy[1], Achebo Joseph[2], Ozigagun Andrew[3], Uwoghiren Frank[4*]
Science and Engineering
[1,2,4]Department of Production Engineering, University of Benin, Benin City, Nigeria
[3]Department of Chemical Engineering, University of Benin, Benin City, Nigeria
Authors' E-mails: timothy.mabiaku@gmail.com, joseph.achebo@uniben.edu, andrew.ozigagun@uniben.edu, frank.uwoghiren@uniben.edu
Corresponding author: Mabiaku T.
Accepted: 1/4/2024 **Published: 16/4/2024**

Abstract: Pipeline welds' structural integrity and strength serve as a cornerstone for ensuring operational safety and effectiveness. Although substantial research has delved into optimizing mechanical properties like yield strength and Young's modulus, a notable gap exists concerning the prediction and enhancement of non-elastic performance factors that substantially influence durability and long-term performance. This research aims to close this gap by scrutinizing the impact of a specific non-elastic factor, namely the Brinell hardness on pipeline weldments. To fulfil this objective, a comprehensive experimental inquiry is conducted, encompassing diverse welding methods, materials, and environmental conditions to authentically replicate real-world situations. The experimental setup adheres to the central composite design, meticulously constructed using design expert software (version 13.0). The Response Surface Methodology analysis yields optimal outcomes, suggesting a current of 160.000 amps, voltage of 21.280 volts, and gas flow rate of 14.667 liters per minute. These parameters collectively yield a welded joint with a hardness of 216.414mpa, achieving a desirability value of 0.918. Additionally, the artificial neural network model is employed to predict output parameters and compared against the RSM methodology, in which the RSM in this case had better predicted values. The findings underscore the pivotal role of optimizing non-elastic performance factors in pipeline weldments. By accurately anticipating and controlling the hardness, engineers and professionals within the pipeline sector can design weldments capable of enduring harsh conditions, curbing the risk of failures, and significantly prolonging pipeline operational lifespans.

Keywords: Hardness, Mechanical properties, Response Surface Methodology, Artificial Neural Network.. Post-harvest loss in tomatoes and tomatillos is a major problem in the market supply chain of small farm holders.

Published by GJEST

1. INTRODUCTION

The integrity of pipeline weldments is a paramount concern in industries where the safe and efficient transportation of fluids is crucial [1]. Among the various factors influencing weldment integrity, hardness plays a pivotal role [2]. Hardness, the ability of a material to resist deformation and penetration, is not merely a mechanical property; it is an indicator of a weldment's strength, durability, and susceptibility to certain forms of degradation [3]. Pipeline weldment integrity is a fundamental concern in industries where the safe and reliable transport of fluids is a necessity [4]. Hardness, a key mechanical property, plays a pivotal contribution to ascertaining the performance and durability of pipeline weldments [5]. This comprehensive literature review delves into the multifaceted importance of hardness, exploring its influence on weldment strength, durability, resistance to deformation, and its crucial role in identifying potential integrity issues.

A material's resistance to deformation, is a vital mechanical property affecting the behaviour of weldments in pipelines, susceptibility to cracking, and resistance to wear and deformation [6]. In pipeline weldments, which are subjected to a range of mechanical stresses, internal pressures, and

environmental conditions, hardness is a key parameter influencing their ability to withstand these challenges [7]. It is not merely a measure of a material's toughness but also serves as an indicator of how a weldment will withstand mechanical stresses, wear, and potential forms of degradation over time. One of the primary reasons for measuring hardness in weldments is to assess weld quality [8]. Properly executed welding processes should result in a uniform hardness profile across the weld zone, with no excessive variations [9]. Deviations from this norm, such as hardness peaks or troughs, can indicate issues like heat-affected zone (HAZ) softening, which may compromise the integrity of the weldment [10].

Hardness in weldments is influenced by various welding parameters, including input of heat, preheating temperature, interphase temperature, and post weld heat treatment (PWHT) [11]. The careful control of these parameters is crucial in maintaining the desired hardness levels, as deviations can lead to hardness-related defects such as hydrogen-induced cracking and embrittlement [12]. The mechanical integrity of pipeline weldments is closely tied to their hardness [13]. Properly controlled hardness levels ensure that the weldments can endure mechanical stresses, including those associated with internal pressure, external loads, and thermal cycling, without experiencing excessive deformation or failure [14]. Hardness also has implications for the susceptibility of pipeline weldments to corrosion [15]. High hardness levels, particularly in heat-affected zones, can render weldments more prone to stress corrosion cracking and hydrogen-induced cracking [16]. Corrosion rates may increase in areas with elevated hardness, potentially compromising the long-term integrity of the pipeline [17]. The relationship between hardness and corrosion in pipeline weldments is a complex one. High hardness levels, particularly in the heat-affected zone (HAZ), can increase susceptibility to certain forms of corrosion, such as stress corrosion cracking. Understanding this relationship is essential for selecting appropriate materials and corrosion mitigation strategies. Hardness is a critical parameter in assessing weld quality [18]. Uniform hardness profiles across a weldment are indicative of a well-executed welding process [19]. Deviations in hardness, such as hardness peaks or troughs, can signal issues such as improper heat input, weld discontinuities, or undesirable microstructural changes, all of which can compromise weldment integrity. Several methods are available for hardness testing in weldments, including Rockwell, Vickers, and Brinell hardness tests [20]. These methods provide quantitative measures of hardness and can be used to identify variations and anomalies within weldments.

2. Findings and Discussion

Process parameters

Twenty experimental runs totaling the current, voltage, and gas flow rate were performed in this study to combine two mild steel plates with dimensions of 60 x 40 x 10 mm. Measurements were made for carbon content, hardness, and % dilution. The process variables taken into account in this research study are the welding current, voltage, gas flow rate in correspondence with the welding pool temperature. Twenty experimental runs totaling the current, voltage, and gas flow rate were performed in this study to combine two mild steel plates with dimensions of 60 x 40 x 10 mm. The Brinell hardness test is conducted using a Brinell hardness testing apparatus. This testing procedure entails the application of a specified force (F) onto a tungsten carbide sphere with a predetermined diameter (D). This force is maintained for a set duration before being released. The spherical indenter imparts a lasting impression or deformation onto the test metal piece. This resulting impression is then measured by averaging two or more diameters to determine the indentation diameter (d). The loading system of the Brinell Hardness Testing Machine, comprising levers, weights, a hydraulic dashpot, and a plunger, encompasses the machine's body. On the movable anvil is kept the test substance. The spherical ball indenter descended on the material using the lever and applied a predetermined force that was shown on the screen.

Materials and experimental set-up

Thermocouples were attached to the process used in gas tungsten arc welding (GTAW). It took place at operating current range of 150 to 200 A, using pure helium as a shielding gas, a DCEN (Direct Current Electrode Negative) with a 4 mm-arc gap was used on a 200 x 200 x 20 mm3 low-carbon steel block. The measured temperatures ranged from 1500 to 1800 °C. The thermocouples were of the tungsten ~W5 variety. The thermocouple's overall diameter, including the tungsten wires and sleeving, was 1.2 mm, and they exhibit good resilience to high temperatures. The thermocouples were inserted into the samples at a depth of 4 mm, 1.4 mm in diameter, and 20° angled. Figure 1 depicts the thermocouple linked to the weld sample.

Modelling and Optimization using Response Surface Methodology (RSM)

The sequential model sum of squares for the hardness response was performed in order to verify that the quadratic model was appropriate for evaluating the experimental data, and the results are shown in Table 1.

Table 1 Sequential model sum of square for hardness

Source	Sum of Squares	df	Mean Square	F-value	p-value	
Mean vs Total	8.803E+05	1	8.803E+05			
Linear vs Mean	1948.22	3	649.41	10.14	0.0006	
2FI vs Linear	9.00	3	3.00	0.0384	0.9895	
Quadratic vs 2FI	**977.41**	**3**	**325.80**	**84.46**	**< 0.0001**	**Suggested**
Cubic vs Quadratic	35.78	4	8.95	19.22	0.0014	Aliased
Residual	2.79	6	0.4654			
Total	8.833E+05	20	44164.70			

The sequential model sum of squares table illustrates how the model fit becomes better as more terms are added. Based on the estimated sequential model sum of squares, the highest order polynomial that has significant additional terms and a model that is not aliased was selected as the best fit. The cubic polynomial was found to be aliased from the findings in table 1, hence it cannot be used to fit the final model. Additionally, it was suggested that the quadratic and 2FI model suited the data the best, which supported the adoption of the quadratic polynomial in this research.

For each, the lack of fit test answer was estimated in order to assess how effectively the experimental data's underlying variation can be explained by the quadratic model. A model with a major fit problem cannot be used to make predictions. Table 2 displays the computed results of the lack of fit for the hardness.

Table 2 Lack of fit test for hardness

Source	Sum of Squares	Df	Mean Square	F-value	p-value	
Linear	1024.98	11	93.18	2.27	0.1856	
2FI	1015.98	8	127.00	2.38	0.1733	
Quadratic	38.58	5	7.72	**0.1406**	**0.9956**	**Suggested**
Cubic	2.79	1	2.79	0.3958	0.6925	Aliased
Pure Error	0.0000	5	0.0000			

Table 3 shows the model statistics for the hardness response that were computed using the model sources

Table 3 Model summary statistics for hardness

Source	Std. Dev.	R^2	Adjusted R^2	Predicted R^2	PRESS	
Linear	8.00	0.6553	0.5906	0.4825	1538.61	
2FI	8.84	0.6583	0.5006	0.2330	2280.52	
Quadratic	**1.96**	**0.9870**	**0.9753**	**0.9004**	**296.07**	**Suggested**
Cubic	0.6822	0.9991	0.9970	0.7930	615.50	Aliased

The standard deviation, R-squared, adjusted R-squared, predicted R-squared, and predicted error sum of squares (PRESS) for each entire model statistics are displayed in the summary statistics of model fit. The ideal criteria for identifying the optimal model source are a low standard deviation, R-Squared close to one, and a relatively low PRESS. The quadratic polynomial model was chosen for this investigation since, according to the results of Table 3, it was indicated whereas the cubic polynomial model was aliased. The goodness of fit statistics shown in Table 4 can be used to confirm that the quadratic model is adequate according to its capacity to decrease the hardness.

Table 4 Goodness of fit statistics for hardness

Std. Dev.	1.96	**R^2**	0.9870
Mean	209.80	**Adjusted R^2**	0.9753
C.V. %	0.9362	**Predicted R^2**	0.9004
		Adeq. Precision	31.6503

The difference between the Predicted R2 of 0.9004 and the Adjusted R2 of 0.9753 is less than 0.2, indicating that they are reasonably in agreement. Adeq Precision measures the signal-to-noise ratio. The ideal ratio is at least 4. Your ratio of 31.650 indicates that your signal is sufficiently strong. Use this model to navigate the design area.

To identify values or groups of values that the model would not have been able to easily identify, a comparison between the projected values and the actual values was made. Figure 1 illustrates this comparison with a focus on the hardness, showing how the dots are densely clustered around the fitted line.

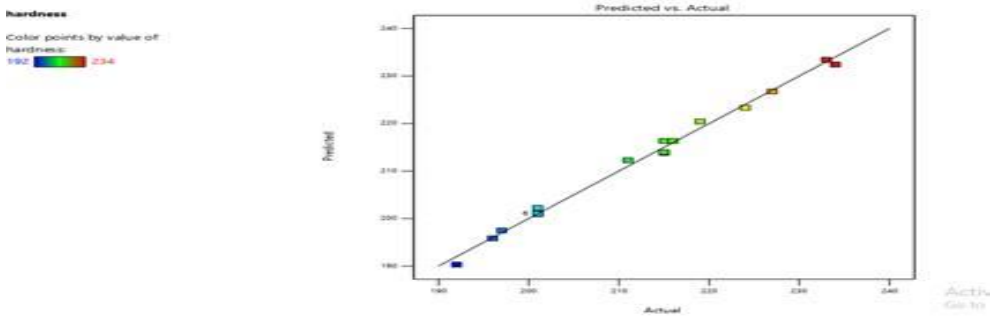

Figure 1 Plot of Predicted Vs Actual for hardne

To search for potential outliers in the experimental data, a Cook's distance plot was made for each response. Cook's distance calculates the potential impact of eliminating a particular point on the regression. Points with extraordinarily high distance values compared to the others should be given additional consideration in order to rule out outliers. The hardness Cook's distance plot is shown in Figure 2.

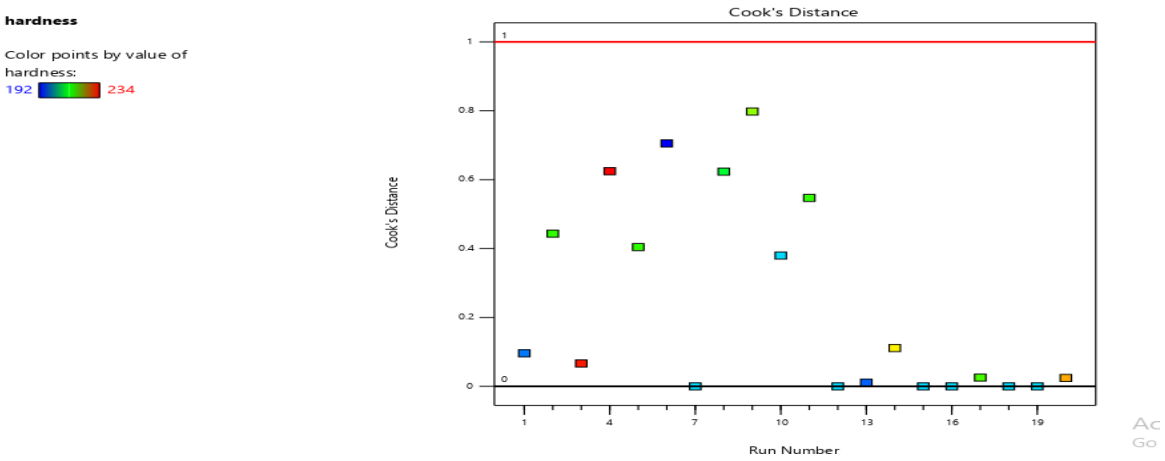

Figure 2 Generated cook's distance for hardness

The Cook's distance plot, which has a lower bound of 0.00 and an upper bound of 1.00, is shown in Figure 2. Experimental results that deviate from the expected range are referred to as outliers and need to be investigated further. The calculated residuals appear to follow a distribution that is roughly normal based on the findings of Figures 1 and 2. This is a positive indication that the accuracy and tendency of the created model for prediction are adequate. Figure 3, 4 and 5 illustrates 3D surface plots created to explore the effects of hardness on gas flow rate, current and voltage. While Figure 6 shows the contour plot of current and voltage.

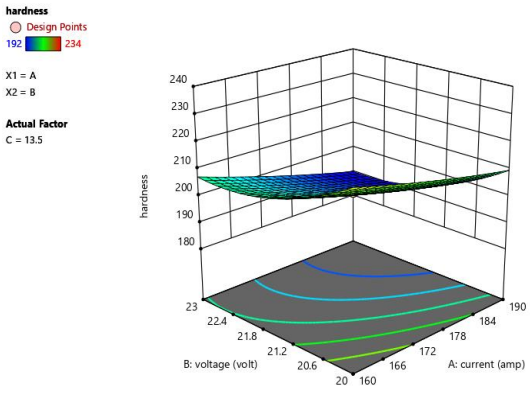

Figure 3 3D Surface plot of current and voltage

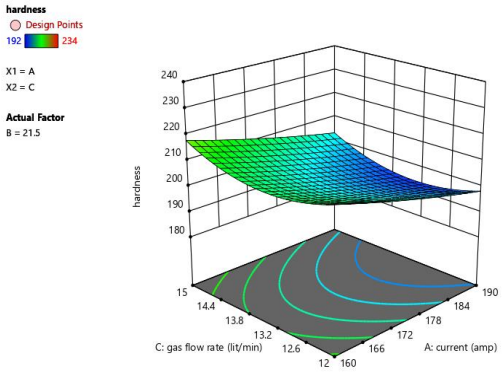

Figure 4 3D Surface plot of gas flow rate and current

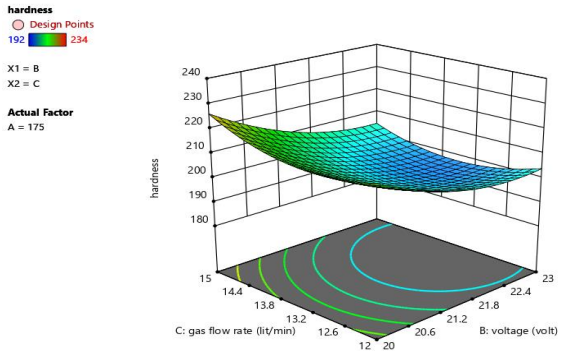

Figure 5 3D Surface plot of current and voltage

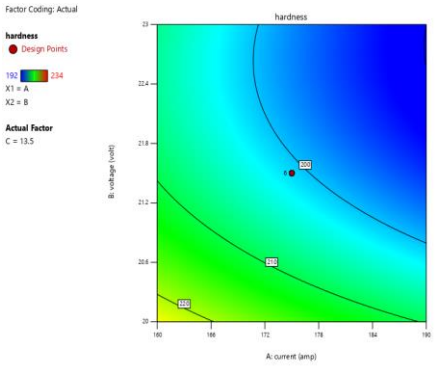

Figure 6 Contour plot of current and voltage

The optimal results of the numerical optimization are shown in Table 5

Table 5 Optimal solutions

S/N		Voltage	Gas flow rate	Hardness	
1	**160.000**	**21.280**	**14.667**	**216.414**	**Selected**
2	160.000	21.286	14.676	216.448	
3	160.000	21.268	14.662	216.462	
4	160.000	21.303	14.690	216.440	
5	160.001	21.259	14.650	216.434	

Modelling of Hardness using Artificial Neural Network (ANN)

The examination also carried substantial significance in establishing a precise mathematical linkage between the response variable (hardness) and the input variables (current, voltage, and gas flow rate). In the pursuit of achieving an optimal network structure that offers the highest degree of accuracy in comprehending the correlation between input and output data, two crucial considerations were taken into account. Firstly, the initial focus encompassed the selection of the most precise training algorithm or learning rule. Secondly, the evaluation of the number of hidden neurons within the network was also carefully deliberated upon. Guided by these considerations, a diverse array of training algorithms and various quantities of hidden neurons were deliberately chosen and subsequently subjected to rigorous experimentation. The overarching objective revolved around pinpointing the optimal training algorithm and the most suitable number of hidden neurons that, when combined, yield the most precise and efficient network configuration. It's important to note that this selection process hinged upon the assessment of r^2 (coefficient of determination) and MSE (mean squared error) values. For the analysis of the Artificial Neural Network, MATLAB R2022a served as the chosen software platform. The data underwent an initial step where it was stored in a dedicated folder within the MATLAB environment. Subsequently, it was normalized through conversion into a numeric matrix. This normalization process was instrumental in automatically establishing the dataset's range, and the import selection functionality was employed to seamlessly import

the data into the MATLAB environment. The Levenberg-Marquardt Back Propagation training algorithm, recognized as the improved second-order gradient method, has been identified as the optimal learning rule and subsequently employed in shaping the network structure. Specifically, the Levenberg-Marquardt Back Propagation training algorithm, configured with 2 hidden neurons, was utilized to train a network comprising one (1) output processing element and three (3) input processing elements (PEs). The choice of employing 2 neurons per layer was maintained, and the network's performance was diligently monitored through coefficients of determination (r^2) and Mean Squared Error (MSE). Within the network architecture, the input layer harnessed the hyperbolic tangent (tan-sigmoid) transfer function to calculate the layer output from input data, while the output layer employed the linear (purelin) transfer function. The process of network generation encompassed the division of input data into training, validation, and testing sets. In this study, 70% of the data was dedicated to network training, 15% for validation, and the remaining 15% for testing. The assessment of the network's performance extended over a maximum of 1000 training epochs. The network underwent training using the "trainlm" function, which systematically updates weight and bias values through the Levenberg-Marquardt optimization process. This particular function is renowned for its efficiency as one of the swiftest back propagation algorithms available. However, it's worth noting that it demands a relatively higher memory footprint compared to other algorithms. By meticulously configuring these parameters and adopting these structural components, an optimal neural network architecture was effectively established. This identical network configuration was then applied to predict hardness as the sole response variable, utilizing three input variables in the process. Visual representation of this network structure is illustrated in Figure 7. The Artificial Neural Network architecture is 3-15-1, the network diagram generated for the prediction of hardness using the back propagation neural network is presented in Figure 8.

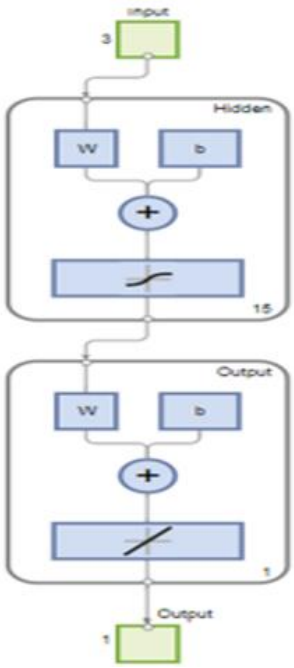

Figure 7 ANN architecture

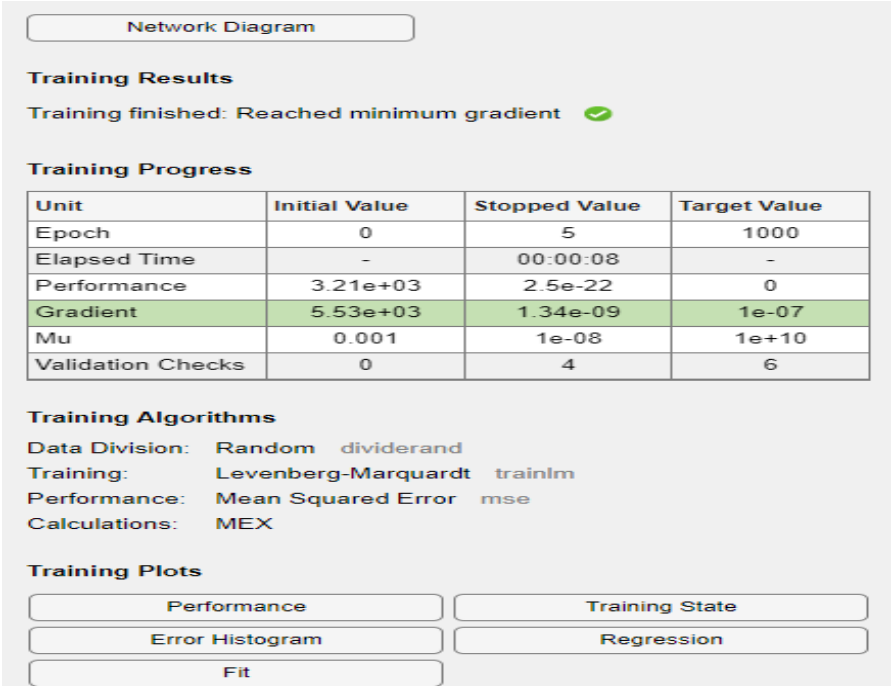

Figure 8 Model summary for predicting hardness

It was noted that the network performance was 3210 from the network training diagram in Figure 8. Out of six (6) validation checks, four (4) were recorded. But given that the issue of weight bias was fixed by normalizing the raw data, this is to be expected. Figure 9 displays a performance evaluation plot that depicts the development of training, validation, and testing. This graphic illustrates the effectiveness of the network at each of these stages.

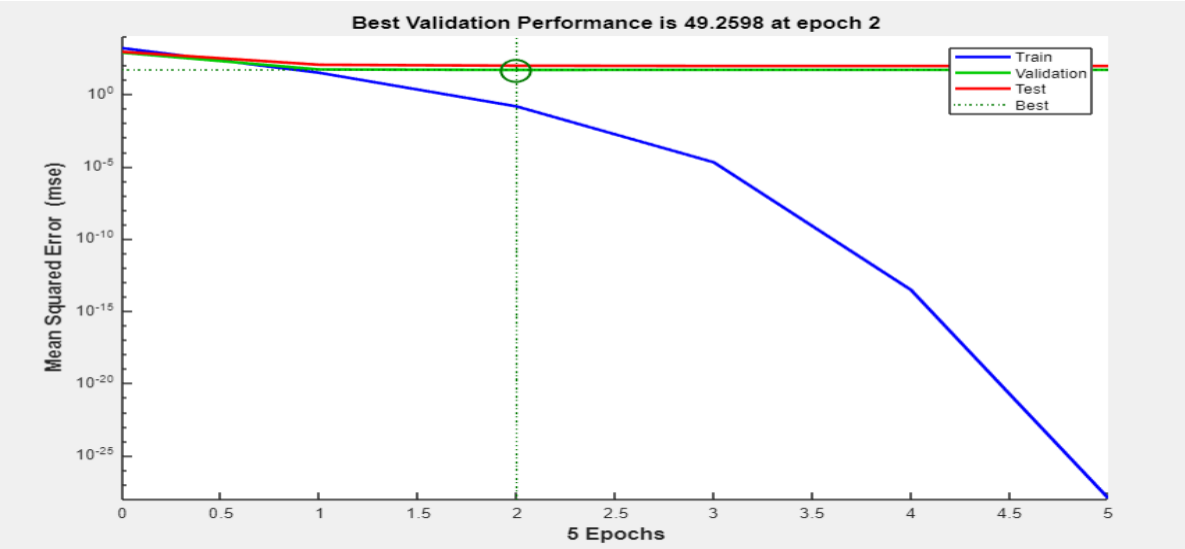

Figure 9 Performance curve of trained network for predicting hardness

Figure 10 depicts the training state and includes information on crucial elements like the gradient function, training gain (Mu), and validation tests. This comprehensive picture allows for a clear understanding of the training process and its related elements.

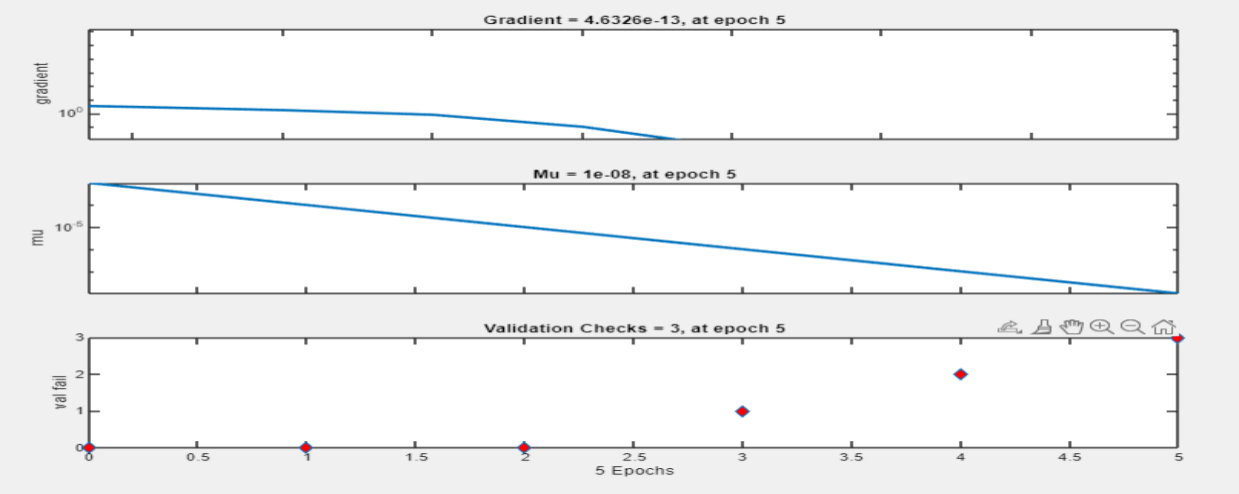

Figure 10 Neural network training state for predicting hardness

In artificial neural networks, back propagation is a technique used to determine each neuron's error contribution following a batch of training data. In order to explain the mistake contributions of each of the chosen neurons, the neural network technically calculates the gradient of the loss function. Better mistake rates. The computed gradient value of 4.6326e-13, as can be shown in Figure 10,

suggests that each selected neuron's error contributions are quite small. The control parameter for the algorithm used to train the neural network is called momentum gain (Mu). Gains from training must have a value that is smaller than unity. Momentum gain of 1e-08 indicate a network with a strong ability to predict the hardness. Momentum increases of 1e-08 indicate a network with a strong ability to predict the hardness. Computed values of the correlation coefficient (R) is shown in Figure 11.

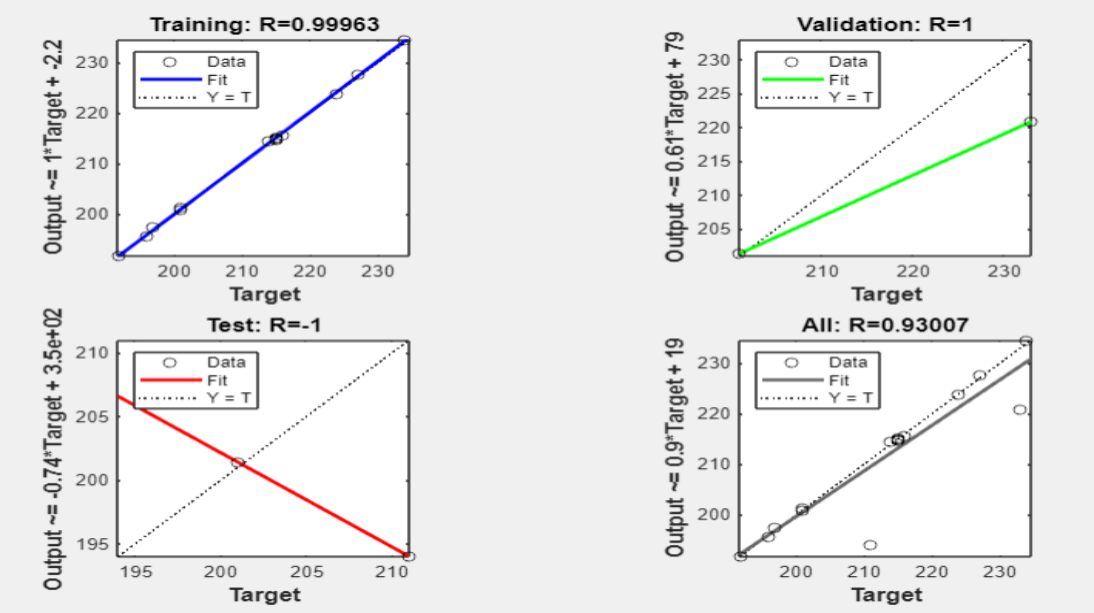

Figure 11 Regression plot showing the progress of training, validation and testing

5. CONCLUSION

In the present study, both Response Surface Methodology (RSM) and Artificial Neural Network (ANN) methods to optimize and predict the hardness of Tungsten Inert Gas (TIG) mild steel welds. Current, voltage, and gas flow rate were taken into consideration as input factors, while the response variable of interest was the hardness. The analysis revealed a quadratic a connection between the input parameters and the outputs, as indicated by the sequential sum of square test for all the responses. The quadratic model exhibited a very low p-value (< 0.0001), confirming its statistical significance. The model summary statistics further underscored the effectiveness of the chosen models. The coefficient of determination (R^2) values for all the responses were consistently around 90%, indicating a strong correlation between the input variables and the predicted responses. Moreover, the models displayed no significant lack of fit, as evidenced by p-values exceeding 0.005. These findings collectively emphasize the robustness of the models in capturing the connection between the response and input parameters. The high R^2 values (> 0.9) across all models demonstrate the strength of the predictive capability of the models. This suggests that the models are highly effective in estimating the selected input variables' values, thereby facilitating the prediction of optimal response values for achieving high-quality welds. Additionally, the variance inflation factor (VIF) of 1.00, which aligns with expectations, signifies that multicollinearity among the input variables is not a concern in this analysis. Overall, the study leveraged both RSM and ANN techniques to create predictive models for hardness in TIG mild steel welds. The findings highlight the models' robustness, with strong correlations, low p-values,

and minimal multicollinearity, all of which contribute to their ability to facilitate the achievement of high-quality welds.

This study uses artificial neural networks and response surface methodology to build numerical models that optimize and predict hardness while taking inputs like current, voltage, and gas flow rate into account. The experimental design employed in this study was the central composite design, generated using Design Expert software version 13.0. Through Response Surface Methodology (RSM) analysis, the study arrived at optimal conditions. These conditions included a current of 160.000 amps, a voltage of 21.280 volts, and a gas flow rate of 14.667 litres per minute. Under these optimized parameters, a welded joint was achieved with a hardness of 216.414 MPa, and this outcome corresponded to a desirability value of 0.918.

In addition to RSM, an Artificial Neural Network (ANN) model was also utilized to predict the output parameters and subsequently compared with the results obtained through RSM methodology. Following a thorough analysis of the outcomes, it was concluded that the response surface methodology outperformed the Artificial Neural Network in terms of predictive accuracy. This determination was based on the observation that RSM yielded a higher coefficient of determination (R^2), signifying its superior predictive capability.

Conclusively, this study employed a central composite design generated via Design Expert software to optimize welding conditions. RSM analysis identified the ideal parameters resulting in a welded joint with a desired hardness value. Furthermore, the study contrasted RSM with an Artificial Neural Network for predictive modelling, ultimately favouring RSM due to its superior coefficient of determination.

6. References

[1] Biezma, M., Andrés, M. A., Agudo, D., Briz, E. (2020). Most fatal oil & gas pipeline accidents through history: A lessons learned approach. Engineering failure analysis, 110, 104446.

[2] Sun, Y., Hamelin, C., Vasileiou, A., Xiong, Q., Flint, T., Obasi, G., Francis, J. and Smith, M. (2020) Effects of dilution on the hardness and residual stresses in multipass steel weldments. International Journal of Pressure Vessels and Piping, 187, p.104154.

[3] Lang, R. (2022). Master of Philosophy Characterizing Containment Weld Integrity for Product Storage Cans (Doctoral dissertation, University of Manchester).

[4] Abdullah, M. and Rahmad, A. (2020). Selection of right inspection tool for challenging pipeline. In Offshore Technology Conference Asia. OnePetro.

[5] Zhang, P., Laleh, M., Hughes, T., Marceau, R., Hilditch, T., & Tan, M. (2023) Effect of Microstructure on Hydrogen Embrittlement and Hydrogen-Induced Cracking Behaviour of a High-Strength Pipeline Steel Weldment.

[6] Muhayat, N., Matien, Y. A., Sukanto, H., Saputro, Y. C. N. (2020). Fatigue life of underwater wet welded low carbon steel SS400. Heliyon, 6(2).

[7] Singh, J. (2021). A Review on Mechanisms and Testing of Wear in Slurry Pumps, Pipeline Circuits, and Hydraulic Turbines. Journal of Tribology, 143(9), 090801.

[8] Richmire, S., Hall, K., Haghshenas, M. (2018). Design of experiment study on hardness variations in friction stir welding of AM60 Mg alloy. Journal of Magnesium and Alloys, 6(3), 215-228.

[9] Li, G., Zhou, L., Luo, S., Huang, Y., Guo, N., Zhao, H., Song, X. (2019). Effect of self-reacting friction stir welding on microstructure and mechanical properties of Mg-Al-Zn alloy joints. Journal of Manufacturing Processes, 37, 1-10.

[10] Khan, M. (2023). Improving the multiscale morphological and mechanical properties of laser welded Al-Si coated 22MnB5 press-hardened steels.

[11]Sharma, A., Verma, D., Kumaran, S. (2018). Effect of post weld heat treatment on microstructure and mechanical properties of Hot Wire GTA welded joints of SA213 T91 steel. Materials Today: Proceedings, 5(2), 8049-8056.

[12] Rizwan, M. (2021). The behaviour of advanced quenched and tempered steels during arc welding and thermal cutting.

[13] Maurya, A., Chhibber, R., Pandey, C. (2023). GTAW Dissimilar Weldment of sDSS 2507 and Nickel Alloy for Marine Applications: Microstructure–Mechanical Integrity. Metallurgical and Materials Transactions A, 1-30.

[14] De Leon, M., and Shin, H. (2022). Review of the advancements in aluminum and copper ultrasonic welding in electric vehicles and superconductor applications. Journal of Materials Processing Technology, 307, 117691.

[15] Sun, Y. and Cheng, Y. (2021). Hydrogen permeation and distribution at a high-strength X80 steel weld under stressing conditions and the implication on pipeline failure. International Journal of Hydrogen Energy, 46(44), 23100-23112.

[16] Hudgins, A., Roepke, C., James, B., Kondori, B., & Whitley, B. (2021). Failures of Pipelines.

17. Bagha, P., Khakbiz, M., Sheibani, S., Hermawan, H. (2018). Design and characterization of nano and bimodal structured biodegradable Fe-Mn-Ag alloy with accelerated corrosion rate. Journal of Alloys and Compounds, 767, 955-965.

[18] Nadimi, N., Pouranvari, M., Ansari, R., Pouranvari, M. (2023). Understanding Fusion Zone Hardness in Resistance Spot Welds for Advanced High Strength Steels: Strengthening Mechanisms and Data-Driven Modeling. Journal of Materials Research and Technology.

[19] Kumar, A., Khadeer, S., Rajinikanth, V., Pahari, S., Kumar, B. (2021). Evaluation of bond interface characteristics of rotary friction welded carbon steel to low alloy steel pipe joints. Materials Science and Engineering: A, 824, 141844.

[20] Wu, H., Dave, F., Mokhtari, M., Ali, M., Sherlock, R., McIlhagger, A., Tormey, D., McFadden, S., (2022). On the application of Vickers micro hardness testing to isotactic polypropylene. Polymers, 14(9), 1804.